Processing and Application of Ceramics 18 [3] (2024) 290–298
https://doi.org/10.2298/PAC2403290A

Effects of La doping on diffused ferroelectric phase transition, electric and dielectric properties of lead-free $SrBi_2Ta_2O_9$ ceramics

Mohamed Afqir[1,*], Didier Fasquelle[2], Amina Tachafine[2], Mohamed Elaatmani[1], Yingzhi Meng[3], Mohamed Daoud[1]

[1]*Laboratoire des Sciences des Matériaux et optimisation des procédés, Faculté des Sciences Semlalia, Université Cadi Ayyad, Marrakech, Morocco*
[2]*Unité de Dynamique et Structure des Matériaux Moléculaires, Université du Littoral Côte d'Opale, Calais, France*
[3]*Guilin University of Technology, Guilin 541006, China*

Received 26 April 2024; Received in revised form 1 August 2024; Accepted 7 September 2024

Abstract

Citric acid-assisted method was used to synthesize pure polycrystalline La-doped $SrBi_2Ta_2O_9$ powders which were uniaxially pressed and sintered under different conditions. La doping of $SrBi_2Ta_2O_9$ resulted in the shortening of Ta–O bond lengths, but increased the unit cell volume and decreased the crystallite size. The effect of sintering process on dielectric properties was studied in order to find optimal sintering conditions. Dielectric loss, measured at room temperature, increases when sintering temperature rises from 1100 to 1200 °C, as well as when sintering time increases from 6 to 9 h. Thus, further investigation was performed on the sample sintered at 1100 °C for 6 h. The obvious change in ε' around T_C and diffusive phase transition, pronounced for the ceramics with higher La content, were characteristic of the doped ceramics. The diffused ferroelectric phase transition behaviour is caused by structural disorder at the Sr-sites (Sr, Bi and La cations) in the Bi_2O_2 layers and perovskite blocks. The electrical conductivity increases steadily at lower temperatures (below 200 °C), but shows a strong temperature- and frequency-dependent trend at higher frequencies. La-doping decreases conductivity by hindering charge carriers' long-distance mobility.

Keywords: *La-doped $SrBi_2Ta_2O_9$, citric acid assisted synthesis, sintering, electric and dielectric properties*

I. Introduction

The use of lead-based compounds has become more problematic due to their high toxicity, so bismuth-based layered Aurivillius oxides were developed to replace them. The Aurivillius compounds are typically described as being formed by the intergrowth of $(Bi_2O_2)^{2+}$ fluorite types and blocks of perovskite structures. The most well-known compound in the wide family of bismuth-based Aurivillius phases is $Bi_4Ti_3O_{12}$ oxide. Due to their important FRAM (ferroelectric random access memories) applications, the double layer-structured ferroelectrics have received much attention [1].

Previous research showed that dielectric and ferroelectric properties of $SrBi_2Ta_2O_9$ depend on dopant type and content. Thus, stoichiometric $SrBi_2Ta_2O_9$ has the Curie temperature (T_C) of ~300 °C, while it is ~400 °C for Sr-deficient-and-Bi-excess $Sr_{0.8}Bi_{2.2}Ta_2O_9$ [2]. The formation of oxygen vacancies is suppressed, leakage current is reduced and the piezoelectric and ferroelectric properties of Aurivillius compounds are enhanced as a result of substitution on the Sr-site [3]. The replacement of transition metal ions on the Ta-site, such as vanadium, results in improved ferroelectric properties [4]. Bringing into structure rare earth cations can improve the intrinsic properties of $SrBi_2Ta_2O_9$. Among them, ion doping on the Bi-site is an effective method to optimize optical properties by introducing Sm^{3+} or Eu^{3+} ions in the lattice [5,6]. It was reported that Bi_2O_2 layer doped with rare earth ions raises the $SrBi_2Ta_2O_9$ remnant polarization [7,8]. However, it has not yet been extensively researched how the rare earth (RE) substitu-

*Corresponding author: tel: +212 701231987
e-mail: *mohamed.afqir@yahoo.fr*

tion at the Bi_2O_2 layer affects the electrical properties of $SrBi_{2-x}RE_xTa_2O_9$ ceramics. In addition, selecting an appropriate processing route is very important. Thus, sintering can considerably enhance densification and grain refinement if optimal conditions are used.

Even though $SrBi_2Ta_2O_9$ materials have been the subject of numerous articles, unleashing the potential of rare earth element dopants for enhancing the dielectric properties is still not deeply discussed in literature reviews. In this work, there are three parts. The first, experimental section, describes a procedure for preparation of five doped $SrBi_2Ta_2O_9$ samples by replacing Bi with La cations. In the second, structural characterization by XRD, FTIR and SEM is presented. Finally, the study of electric and dielectric properties as well as corresponding physical models, reflecting the influence of doping, is presented in the third section.

II. Experimental

Two steps were required to prepare polycrystalline La-doped $SrBi_2Ta_2O_9$ powders labelled as SBT-0, SBT-1, SBT-2, SBT-3 and SBT-4 containing 0, 0.28, 0.69, 1.03 and 1.38 at.% of La, respectively (Table 1). In the first step, $SrCO_3$ (Labosi), Ta_2O_5, La_2O_3 (Riedel-de Haën, 99%) and Bi_2O_3 (Rectapur, 99%) were weighed according to the stoichiometry. Then the powders were homogenized and stirred for 30 min in a beaker with citric acid (CA) and a small amount of nitric acid (NA) with volume ratio 2:0.1 (CA:NA). The obtained mixture was calcined at 500 °C for 24 h. The solid-state reaction process is used in the second step. The resulting powder was calcined at 1000 °C (selected as the optimal calcination temperature) for 8 h. The calcined powders were uniaxially pressed (2 t) and sintered at various temperatures (1100 and 1200 °C) for various times.

To follow the conversion of reactants into desired products, XRD (Rigaku) was used. Scanning electron microscope (SEM, TESCAN) and energy-dispersive X-ray spectroscopy (EDX) measurements were performed using an EDAX analyser (TESCAN). Fourier transform infrared spectroscopy (FTIR, Bruker, Vertex 70 DTGS) was performed by KBr-pellet method. The sintered pellets were burned in air for 20 min at 400 °C with silver paste electrodes applied to both sides. At room temperature, the Solartron 1260 impedance/gain-phase analyser and Agilent 4284A were used to test the dielectric properties as a function of frequency.

III. Results and discussion

3.1. Structural characterization

Figure 1 shows XRD patterns of the undoped and La-doped $SrBi_2Ta_2O_9$ calcined powders. All synthesized compounds were matched with $SrBi_2Ta_2O_9$ structure from the standard reference database (PDF# 01-089-6490). The variations in cell volume and the lattice parameters a, b and c (Table 1) show that the unit cell is locally distorted in the case of La doping. Consequently, when La content increased, the unit cell volume and lattice parameters c and b increased, but there was no obvious change of a. In comparison to Bi^{3+}, La^{3+} has a larger ionic radius, i.e. Bi^{3+} has ionic radius of 1.02 Å and 1.11 Å for coordination numbers VI and VIII, compared to 1.061 Å and 1.18 Å for La^{3+}, respectively. Thus, the differences in ionic radii may be the primary reason for the variations in lattice parameters. In addition, the orthorhombicity $(a-b)/(a+b)$ ratio decreases with La-doping (Table 1), suggesting that the perovskite-part structure of the undoped sample has a more distorted orthorhombic structure. The crystal-

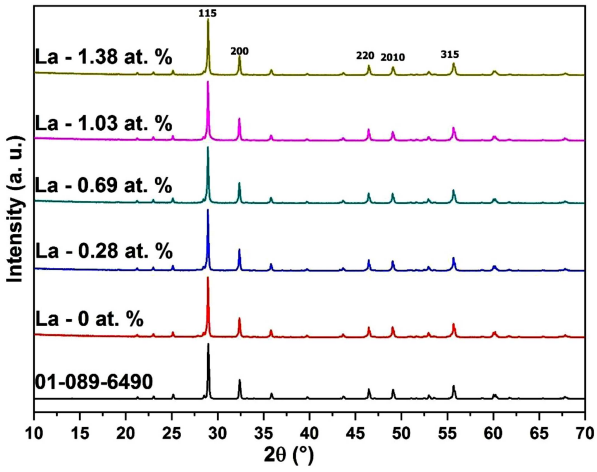

Figure 1. XRD patterns of La-doped $SrBi_2Ta_2O_9$ ceramic powders

Table 1. Structural characteristics (obtained from XRD and FTIR) of calcined powders

Sample	SBT-0	SBT-1	SBT-2	SBT-3	SBT-4
La content [at.%]	0	0.28	0.69	1.03	1.38
a [Å]	5.5926	5.5904	5.5912	5.5941	5.5929
b [Å]	5.5866	5.5879	5.5880	5.5884	5.5907
c [Å]	25.3277	25.3346	25.3385	25.3497	25.3508
Cell volume [Å^3]	791.32	791.42	791.66	792.47	792.68
Crystallite size [nm]	81.5	89.1	72.7	74.0	56.2
$(a-b)/(a+b)$	0.00053	0.00022	0.00029	0.00051	0.00020
k [N/m]	343.32	346.19	344.97	346.39	347.83
l [Å]	1.7044	1.6997	1.7017	1.6994	1.6971

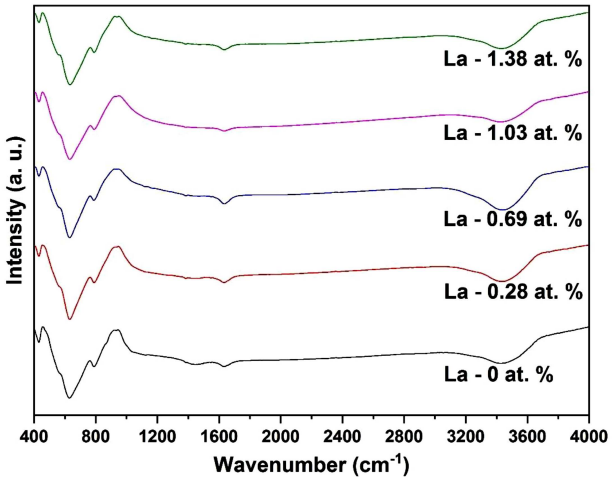

Figure 2. FTIR spectra of La-doped $SrBi_2Ta_2O_9$ ceramic powders

lite size values of the SBT-0 and SBT-1 samples are 81.5 and 89.1 nm, respectively, and there is a decrease to 56.2 nm when the La content in the structure reaches 1.38 at.% (Table 1).

Figure 2 shows the FTIR spectra of the La-doped $SrBi_2Ta_2O_9$ powders. The distinctive $SrBi_2Ta_2O_9$ bands may appear between 400 and 930 cm^{-1}. Ta–O vibration within the TaO_6 octahedron is responsible for the peaks that appear at 526, 596 and 954 cm^{-1} [9]. The bands observed above 1200 cm^{-1} could be attributed to the overall amount of suspended organic matter and humidity.

By assuming that the atoms are point masses connected by a spring that obeys Hook's law and has a constant force we obtain the equation:

$$k = 4\pi^2 \frac{c^2 \cdot \bar{\nu}^2 \cdot \mu}{N_A} \tag{1}$$

where c, $\bar{\nu}$, N_A and μ are velocity, wavenumber, the Avogadro number and reduced mass respectively. Using the force constant, the following expression could be used to estimate Ta–O bond length (l) [10]:

$$k = \frac{17}{l^3} \tag{2}$$

According to this calculation (Table 1), the partial occupancy of Bi^{3+} by La^{3+} leads to the shorter Ta–O bond, enhancing the bond strength and giving rise to the vibration mode at higher wavenumbers: 629.48, 632.11, 630.99, 632.29 and 633.6 cm^{-1} for the samples SBT-0, SBT-1, SBT-2, SBT-3 and SBT-4, respectively. In the undoped sample, the Ta–O bond length (1.7044 Å) is smaller than in the doped ceramics. Thus, the Rietveld refinement data showed that the four distinct Ta–O bond lengths cause the TaO_6 octahedron to become less symmetrical [11]. This set of Ta–O bond lengths shows a reduction as a result of the La doping.

Figure 3 shows SEM images of the fractured surface of the ceramics sintered at 1100 °C for 6 h. It has been shown that when the compounds were synthesized via the solid-state technique, ceramic microstructure is characterized by the formation of plate-like grains [8,12]. According to SEM analyses plate-like structure is not clearly visible, and there is no significant difference in the microstructures of the prepared samples. It seems that the undoped sample shows tightly packed small and large grains, whereas the sample SBT-4 with 1.38 at.% of La contains only small grains (smaller than 1.5 μm).

3.2. *Dielectric measurements*

Effect of sintering conditions

The effect of the sintering process on dielectric properties was studied in order to come up with the optimal conditions regarding temperature and time of sintering. Figure 4a shows dialectic loss versus frequency of the undoped $SrBi_2Ta_2O_9$ ceramics measured at room tem-

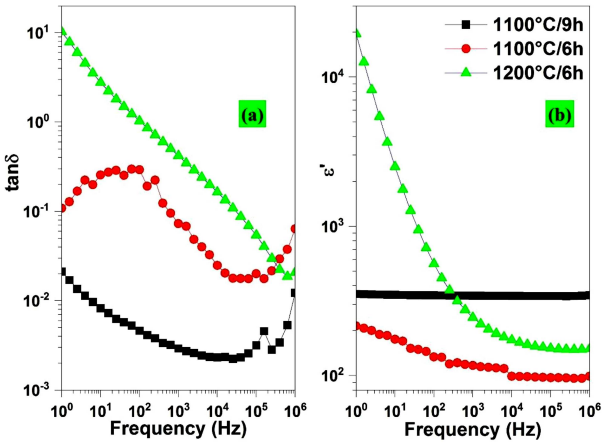

Figure 4. Influence of sintering conditions of undoped ceramics on: a) dielectric loss and b) dielectric constant measured at room temperature

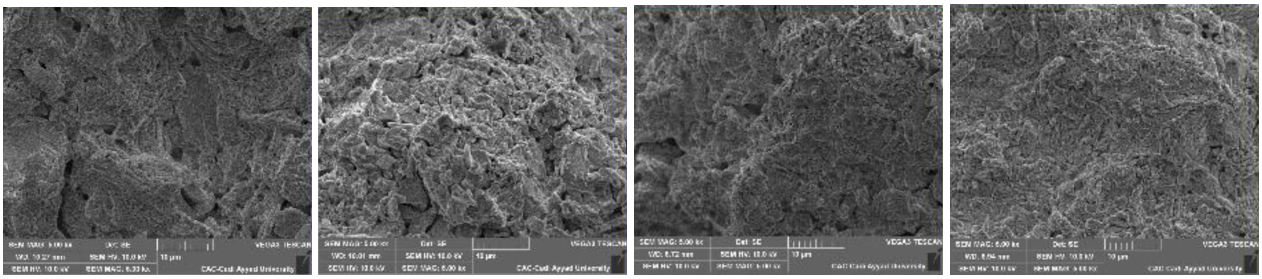

Figure 3. SEM images of $SrBi_2Ta_2O_9$ ceramics: a) SBT-0, b) SBT-2, c)SBT-3 and d) SBT-4

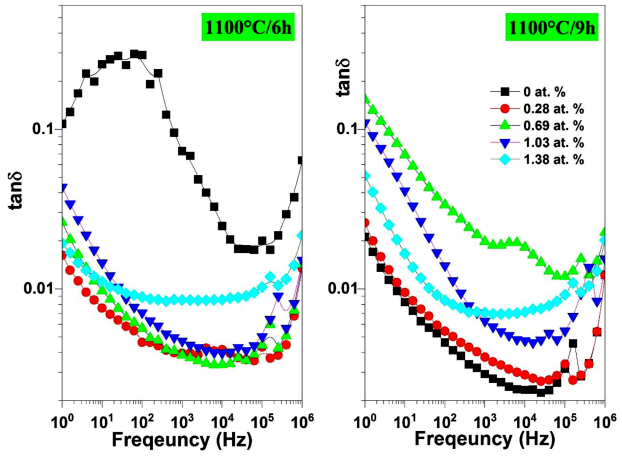

Figure 5. Influence of sintering time on dielectric loss measured at room temperature of La-doped $SrBi_2Ta_2O_9$ ceramics

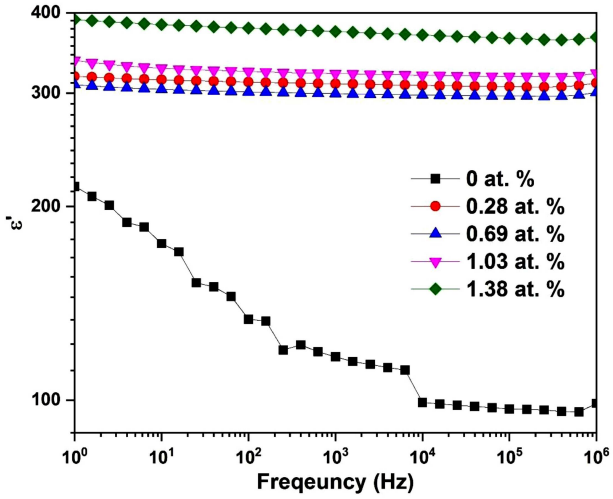

Figure 6. Dielectric constant of La-doped $SrBi_2Ta_2O_9$ ceramics sintered at 1100 °C/6 h as a function of frequency

perature. Dielectric loss increases as sintering temperature rises. Thus, dielectric loss increased to reach 0.4 for the ceramics sintered at 1200 °C, whereas it decreased to 0.002 (at 1 kHz) for the ceramics sintered at 1100 °C. Meanwhile, with extended time of sintering, dielectric loss decreases significantly. At 1 kHz, tan δ drops from 0.07 to 0.02 after 6 h and 9 h of sintering at 1100 °C, respectively.

The dielectric constant (ε') of the undoped $SrBi_2Ta_2O_9$ ceramics has remarkable change as a result of the changed sintering conditions (Fig. 4b). It is assumed that the accumulation of charges at grain boundaries of the sample sintered at 1200 °C is the reason why the value of ε' is higher at lower frequencies and decreases steeply. This dielectric constant trend disappears for the ceramics sintered at 1100 °C. It is interesting that the dielectric constant of the ceramics sintered at 1100 °C/9 h is almost constant in the whole frequency range (from 1 Hz to 1 MHz), which could be caused by the high ceramics density. Thus, it was found that the dielectric constants at 10 kHz are 342, 99 and 173, for the ceramics sintered at 1100 °C/9 h, 1100 °C/6 h and 1200 °C/6 h, respectively.

Figure 5 compares the dielectric loss measured at room temperature for the La-doped $SrBi_2Ta_2O_9$ ceramics sintered at 1100 °C for various times. The dielectric loss of the doped samples is smaller than that for the undoped ceramics sintered at 1100 °C for 6 h. Thus, the dielectric loss at 1 kHz falls from 0.07303 for the undoped sample (SBT-0) to 0.00395, 0.00385, 0.00471 and 0.00851 for the SBT-1, SBT-2, SBT-3 and SBT-4 ceramics. However, the La-doping deteriorates the dielectric loss for the ceramics sintered at 1100 °C for 9 h and the tan δ values increase with La content. Thus, tan δ at 1 kHz is approximately 0.0029 for the undoped sample and increased to 0.019 when 0.96 at.% of La was added. As a result of the variation in the samples' sintered densities as a function of sintering temperature, results show that sintering circumstances have a significant impact on dielectric properties (Fig. 5).

According to the presented results it seems that optimal sintering conditions are: i) sintering temperature of 1100 °C and ii) dwell time of 6 h. Thus, change of ε' with frequency for the ceramics sintered at 1100 °C for 6 h were performed and the obtained results are shown in Fig. 6. The dielectric constant of the La-doped sample sintered at 1100 °C for 6 h is almost constant in the whole frequency range, similar to the case of the undoped SBT ceramics sintered at 1100 °C for 9 h. Higher La amount, incorporated into the lattice structure, increases the dielectric constant. Thus, the dielectric constant at 1 kHz and room temperature of the sample SBT-4 with 1.38 at.% La ($\varepsilon' \sim 374$) is three times higher than that of the undoped sample ($\varepsilon' \sim 117$).

Temperature dependent dielectric properties

Figure 7 displays how dielectric constant (ε') and dielectric loss (tan δ) change with La content in five samples sintered at 1100 °C for 6 h. It is clear that the dielectric constant rises up to the Curie temperature (T_C) and then decreases. However, there is an obvious change in ε' around T_C and the diffusive phase transition is pronounced for the ceramics with higher La content. The ferro-paraelectric transition temperature (T_C) decreases as a result of introducing La into the lattice structure. The Curie temperature (Table 2) decreases from 311 °C for the undoped sample to 302, 283 and 210 °C for the samples with 0.28, 0.69 and 1.38 at.% of La, respectively, due to the distortion of the unit cell. Based on these results, La addition can vary the rate at which Ta^{5+} ions oscillate within the TaO_6 octahedron in the perovskite-part lattice. As more La^{3+} ions are introduced into the lattice, Ta^{5+} oscillation process becomes slower, which causes T_C to decrease. Reduced ferroelectric transition temperatures are associated with lower orthorhombicity.

However, T_C increased when the La content rose to 0.69 at.% for two reasons. The first, La has a relatively larger ionic radius despite the fact that the ionic radii

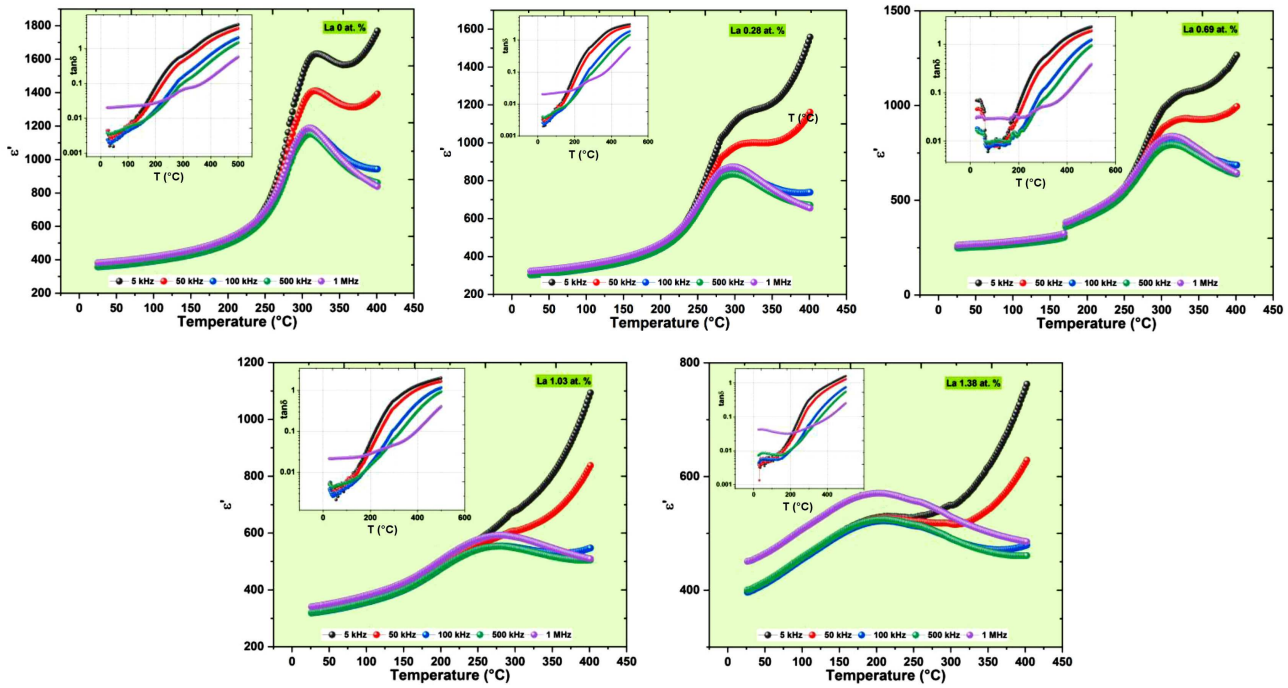

Figure 7. Dielectric constant (ε') and dielectric loss ($\tan\delta$) of La-doped $SrBi_2Ta_2O_9$ ceramics sintered at 1100 °C/6 h as a function of frequency and temperature

Table 2. Electric and dielectric properties of doped samples

Sample	La content [at.%]	T_C [°C]	ε'_{max} at T_C at 1 MHz	γ	ε' at RT and 1 kHz	$\tan\delta$	σ_{AC} [S/m] at 50 kHz at 50 °C	at 400 °C
SBT-0	0	311	1188	0.86	343	0.0029	2.24×10^{-5}	0.0017
SBT-1	0.28	302	872	0.97	336	0.0037	1.24×10^{-5}	0.0014
SBT-2	0.69	315	838	1.12	289	0.0198	4.10×10^{-6}	7.23×10^{-4}
SBT-3	1.03	283	592	1.26	328	0.0063	1.42×10^{-6}	6.32×10^{-4}
SBT-4	1.38	210	570	1.51	346	0.0071	3.25×10^{-6}	2.73×10^{-4}

of Bi and La are extremely similar. It could be possible that 0.69 at.% of La in $SrBi_2Ta_2O_9$ has optimum lattice distortion, which is the cause of a compressive stress resulting in the increase in T_C. It is noted that the trend in T_C is also consistent with the orthorhombicity. The second, the increase of T_C arises from the distribution of La between the Bi and Sr sites, changing the Sr vacancies' content as well.

As shown in Table 2, the dielectric constant decreased with increasing La concentration and it is due to the effect of $6s^2$ lone pair of Bi^{3+} ion [13,14].

The temperature dependence of $\tan\delta$ (Fig. 7) exhibits two distinctive temperature ranges. In the first range, 25–200 °C, $\tan\delta$ was consistently below 7×10^{-3}. However, in the second range, 200–400 °C, $\tan\delta$ rises sharply to reach 0.1 at 300 °C, indicating an increase in charge transfer in the samples.

Both 1.03 at.% and 1.38 at.% compounds show exceptional performance since at the transition temperature a wider peak than in other doped samples is more notable. This behaviour, known as a diffused ferroelectric phase transition, typically results from changes in composition and cation disorder at the same crystallographic location. The modified Curie-Weiss law allows for a significant evaluation of the phase transition's degree of diffuseness:

$$\frac{1}{\varepsilon'} - \frac{1}{\varepsilon'_{max}} = \frac{(T - T_m)^\gamma}{C} \tag{3}$$

where γ and C are constants and T_m is the transition temperature at which the dielectric constant is the highest (ε'_{max}). The normal Curie-Weiss law is obtained when $\gamma = 1$. If an ideal relaxor ferroelectrics were perfect, $\gamma = 2$. In this regard, Fig. 8 illustrates the linear fitting plot of $\ln(1/\varepsilon' - 1/\varepsilon'_{max})$ versus $\ln(T - T_m)$ in order to obtain the γ value from the slop.

The estimated values of the degree of diffusion (γ) are given in Table 2. It is observed that addition of La^{3+} to the $SrBi_2Ta_2O_9$ ceramics increases the diffusive-type phase transition, i.e. γ values were 0.86, 0.97, 1.12, 1.26 and 1.51 for the sample SBT-0, SBT-1, SBT-2, SBT-3 and SBT-4, respectively. It has been reported previously that in both the perovskite and the bismuth layers, the lanthanide ions (Ln^{3+}) substitution also brought the A-site cations' disorder in the double-layer [15,16].

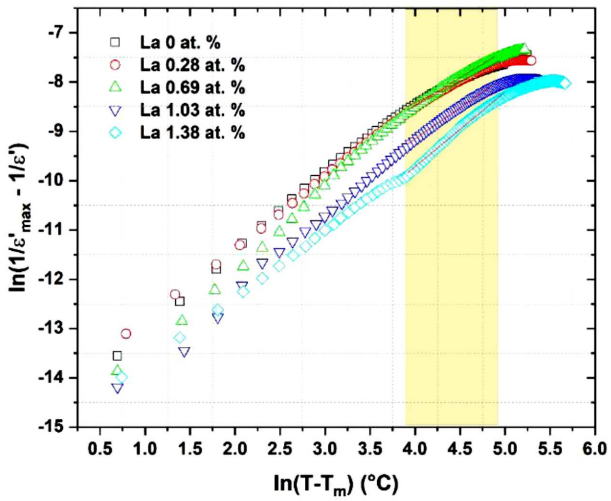

Figure 8. $\ln(1/\varepsilon'-1/\varepsilon'_{max})$ versus $\ln(T-T_m)$ at 1 MHz of La-doped $SrBi_2Ta_2O_9$ ceramics

Figure 9 shows dielectric constant (ε') and dielectric loss ($\tan\delta$) versus frequency at various temperatures. With an increase in temperature, ε' and $\tan\delta$ rapidly increase. This shows that at low frequencies and high temperatures, conduction has a significant impact on ε'. The ε'-plots exhibit substantial low-frequency dielectric dispersion, which may be primarily caused by the response of space charges at low frequency. As the temperature rises and the frequency decreases, the value of $\tan\delta$ increases. The $\tan\delta$-plots do not show any loss peaks, due to the conduction phenomena or/and electrode polarization. Grains and grain boundaries have different properties. Defects in grain boundaries trap the charge carriers, creating a dipole moment. At lower frequencies, the dielectric polarization is caused by charge carriers hopping between defect centres at grain boundaries [17].

Temperature dependent conductivity

Figure 10 shows the AC conductivity as a function of frequency and temperature. Overall, because NTCR (negative temperature coefficient of resistance) is a feature shared by all compounds, conductivity increases exponentially with increasing temperature. The conductivity curves are split into two zones: those that are flat and those that have a positive slope.

Between room temperature and 200 °C, the AC conductivity increased steadily and showed significant frequency dispersion. As a result of the hopping conduction process, AC conductivity increases with frequency.

However, the frequency-dependent conductivity curves merge, while the conductivity values are reversed when the temperature exceeds 300 °C. The undoped sample has a room-temperature AC conductivity of up to 0.224 μS/m (at 50 kHz), which is among the highest of all compounds reported in this work. Accordingly, at 400 °C (50 kHz), the undoped sample has the highest AC conductivity of 1.66 mS/m, while the La 1.38 at.% sample has the lowest with 2.72×10^{-4} S/m.

Furthermore, at high temperatures, charge carrier mobility can have a considerable impact on AC conductivity. A large number of oxygen vacancies have formed, resulting in an undoubtable increase in conductivity. The lanthanum reduces the energy required for the charge carrier to move through the lattice structure, which increases conductivity.

The frequency dependence of the electrical conductivity at various temperatures of the La-doped $SrBi_2Ta_2O_9$ ceramics (Fig. 10) could be divided into two zones. The electrical conductivity in the low-frequency zone (< 10^4 Hz) is frequency-independent and refers to σ_{DC}, which rises with temperature and

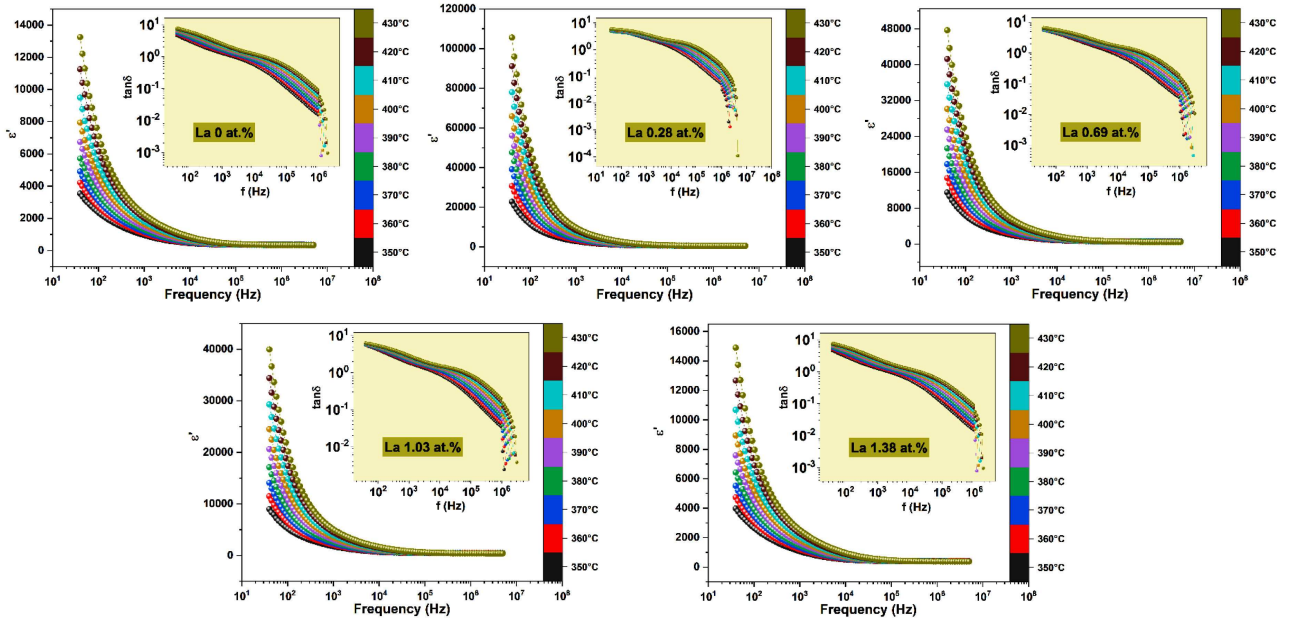

Figure 9. Dielectric constant (ε') and dielectric loss ($\tan\delta$) versus frequency at various temperatures of La-doped $SrBi_2Ta_2O_9$ ceramics

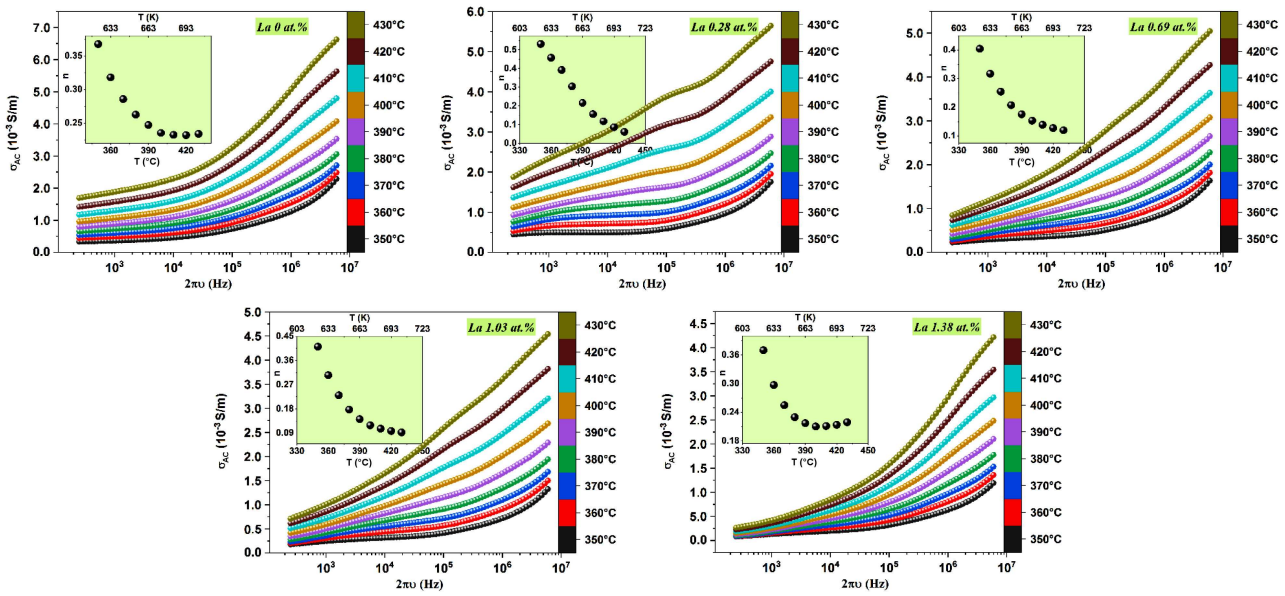

Figure 10. AC conductivity versus frequency at various temperatures of La-doped $SrBi_2Ta_2O_9$ ceramics

causes long-distance motion of the charge carriers. The low-frequency plateau length, however, is temperature-dependent for doped samples. Consequently, as the temperature rises, the length of the plateau shortens.

It is estimated that σ_{DC} values at 370 °C were 3.96×10^{-4}, 7.62×10^{-4}, 2.45×10^{-4}, 1.74×10^{-4} and 3.93×10^{-5} S/m for the doping levels of 0, 0.28, 0.69, 1.03 and 1.38 at.%, respectively. Therefore, a high La-doping level (for example, 1.38 at.%) could hinder charge carriers' long-distance mobility. At higher frequencies, the electrical conductivity shows a strong temperature- and frequency-dependent trend. Thus, as temperature and frequency increase, the conductivity increases more intensively. In this regard, using the Jonscher's power relationship allows us to reveal the mechanism of conduction in the sample.

The electrical conductivity exhibits a considerable frequency- and temperature-dependent behaviour at higher frequencies (> 10^4 Hz). Therefore, conductivity increases in proportion to temperature and frequency. In this regard, utilizing the analytical equation proposed by Jonscher enables an understanding of the sample's conduction mechanism:

$$\sigma = \sigma_{DC} + A(2\pi\omega)^n \tag{4}$$

where A is a constant related to temperature and n is the frequency exponent. Since the frequency exponent decreases as temperature rises, correlated barrier hopping (CBH) is considered to be the most appropriate model. The latter provides the jumps of charge carriers between the neighbouring sites [16,17].

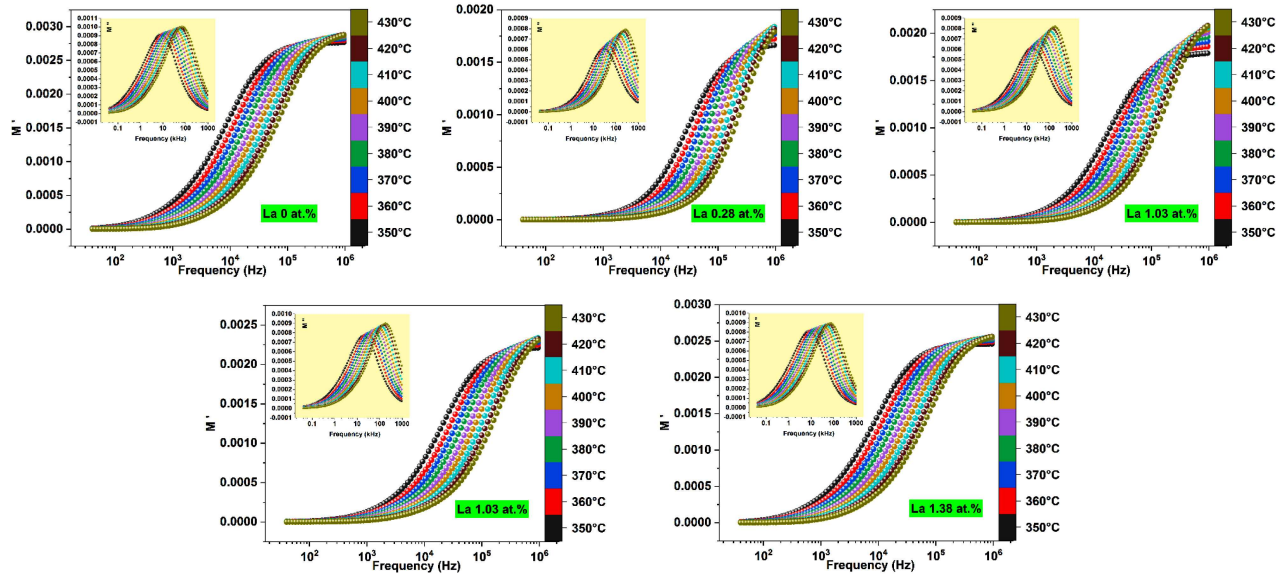

Figure 11. The real (M') and imaginary (M'') parts of the electric modulus of La-doped $SrBi_2Ta_2O_9$ ceramics as a function of frequency at various temperatures

Temperature dependent electrical modulus

The electrical modulus of real (M') and imaginary (M'') parts versus frequency at various temperatures are shown in Fig. 11. The ion conductivity relaxation process of this material results in asymmetrical peaks in M''-graphs. While the maximum M'' values increased as the temperature increased, the La-doping level has little impact on the maximum M'' position. The peak position shifting with temperature suggests that these charge carriers are led by the hopping mechanism [18,19]. Overall, the range in which charge carriers are movable across long distances is determined by the frequency below the peak maximum. The carriers are confined to potential wells and are only movable over short distances at the frequency above the peak.

At low frequencies, all M'-curves seem to converge to zero, indicating that there is no electrode polarization in the samples. The fact that all of the high-frequency curves merge with one another indicates the absence of space polarization (interfacial polarization) [20]. Modulus M' increases gradually with frequency and attains its maximum value at a constant value. This indicates that charge carriers can move over extended distances since their mobility is not constrained by the restoring force [20].

Temperature dependent impedance

The impedance spectra of the prepared samples are shown in Fig. 12. Overall, the first and second arc diameters, which are related to the grain and grain boundary, respectively, get smaller as the temperature rises. The grain resistance (1st arc) is lower than the grain boundary resistance (2nd arc) (Fig. 12a). At 400 °C, the grain resistance decreased from 0.197 MΩ for the undoped sample to 0.0088, 0.070, 0.033 and 0.046 MΩ for the sample with 0.28, 0.69, 1.03 and 1.38 at.% of La, respectively. While the undoped sample exhibits the highest grain boundary resistance values at temperatures between 350 and 370 °C, the grain boundary resistance fluctuates slightly at higher temperatures (>400 °C). Considering that grain resistance is lower than grain boundary resistance, charges on either side of the grain boundary are blocked, forming a potential barrier and obstructing the passage of charge carriers. Therefore, it is possible that the localized charges are what cause the grain conductivity [3,21].

The impedance spectra were analysed by using $R_s(CPE\text{-}R_p)$ equivalent circuit, where R is a resistance and CPE is a constant-phase element (the obtained results are not shown here). Meanwhile, CPE consists of two parameters: capacity ($CPE\text{-}T$) and an exponent ($CPE\text{-}P$). It was shown that the increasing either the temperature or the level of La-doping causes an increase in the grain and grain boundary capacitances ($CPE\text{-}T$).

IV. Conclusions

La-doped $SrBi_2Ta_2O_9$ ceramics were prepared by auto-combustion through citric acid, which is followed by a solid-state reaction and sintering. When the La-doping increased the lattice volume was expanded. The FTIR data revealed that the Ta–O bond length was affected by La doping in a way that caused a reduction. The lowest dielectric loss of the undoped sample was obtained for the ceramics that was sintered at 1100 °C for 9 h. However, it appeared that the ceramics sintered at 1100 °C for 6 h may result in a reduction in dielectric loss when La-doping was introduced. La-doping also results in an increase in the dielectric constant and more pronounced diffusive phase transition. The dif-

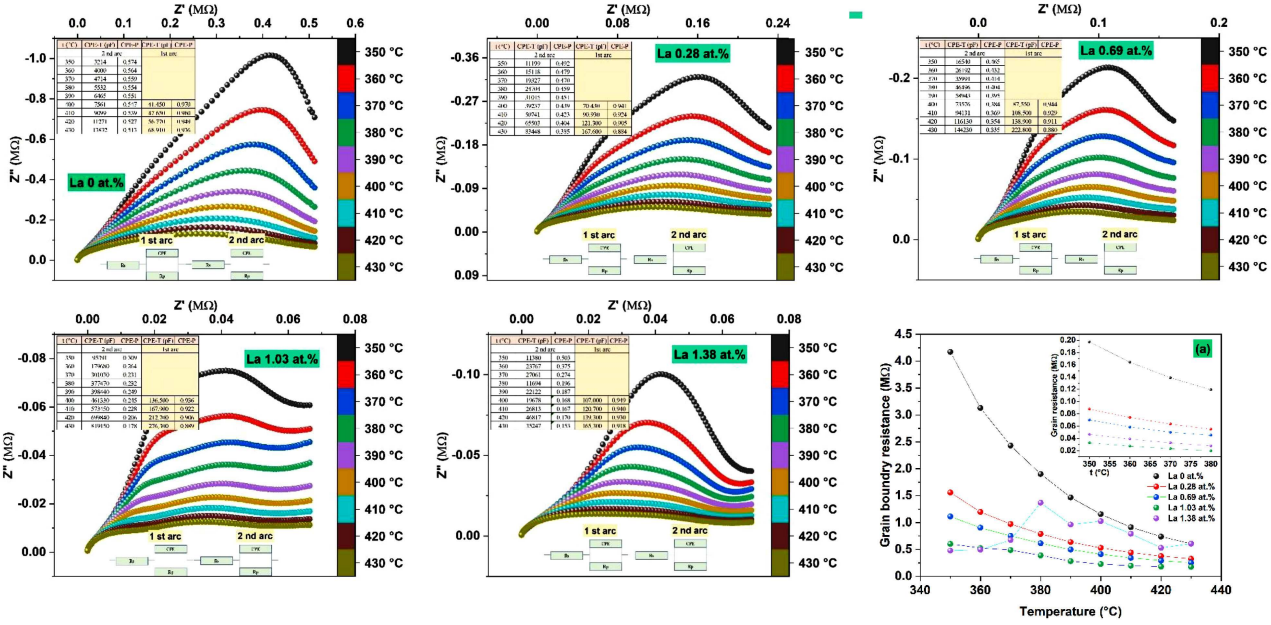

Figure 12. Nyquist plots at various temperatures of La-doped $SrBi_2Ta_2O_9$ ceramics – grain boundary and grain resistances versus temperature (a)

fused ferroelectric phase transition behaviour is caused by structural disorder at the Sr-sites (Sr^{2+}/Bi^{3+}/La^{3+}) in the Bi_2O_2 and perovskite layers. The electrical conductivity increases steadily at lower temperatures (below 200 °C), but shows a strong temperature- and frequency-dependent trend at higher frequencies. La-doping decreases conductivity by hindering charge carriers' long-distance mobility.

References

1. S. Supriya, "Tailoring layered structure of bismuth-based aurivillius perovskites: Recent advances and future aspects", *Coord. Chem. Rev*., **479** (2023) 215010.
2. Y. Shimakawa, Y. Kubo, Y. Nakagawa, T. Kamiyama, H. Asano, F. Izumi, "Crystal structures and ferroelectric properties of $SrBi_2Ta_2O_9$ and $Sr_{0.8}Bi_{2.2}Ta_2O_9$", *Appl. Phys. Lett*., **74** (1999). 1904–1906.
3. V. Senthil, S. Panigrahi, "Dielectric, ferroelectric, impedance and photocatalytic water splitting study of Y^{3+} modified $SrBi_2Ta_2O_9$ ferroelectrics", *Int. J. Hydrogen Energy*, **44** [33] (2019) 18058–18071.
4. C.C. Wu, C.F. Yang, "Effect of V_2O_5 B-site substitution on the microstructure, Raman spectrum, and dielectric properties of $SrBi_2Ta_2O_9$ ceramics", *Sci. Rep*., **10** (2020) 19147.
5. Y. Zhong, B. Deng, X. Gao, P. Sun, Y. Ren, T. Liang, R. Yu, "High thermally Sm^{3+}-activated $SrBi_2Ta_2O_9$ orange-red phosphor: Preparation, characterization, and optical properties", *J. Lumin*., **215** (2019) 116648.
6. Y. Zhong, P. Sun, X. Gao, Q. Liu, S. Huang, B. Liu, B. Deng, R. Yu, "Synthesis and optical properties of new red-emitting $SrBi_2Ta_2O_9$:Eu^{3+} phosphor application for w-LEDs commercially based on InGaN", *J. Lumin*., **212** (2019) 45–51.
7. V. Senthil, T. Badapanda, S. Panigrahi, "Ferroelectric and dielectric study of Y^{3+} substitution at Bi-site on $SrBi_2Ta_2O_9$ ferroelectric ceramic", *AIP Conf. Proc*., **2115** (2019) 030558.
8. V. Senthil, T. Badapanda, A. Chandrabose, S. Panigrahi, "Dielectric and ferroelectric behavior of cerium modified $SrBi_2Ta_2O_9$ ceramic", *Mater. Lett*., **159** (2015) 138–141.
9. I. Bella, T.P. Wendari, N. Jamarun, N. Mufti, Zulhadjri, "Hydrothermal synthesis of $ABi_2Ta_2O_9$ Aurivillius phase: A comparative study of A-site cation size on structure, dielectric, optical properties", *J. Adv. Dielectr*., **12** (2022) 2150031.
10. H. Singh, K.L. Yadav, "Structural, dielectric, vibrational and magnetic properties of Sm doped $BiFeO_3$ multiferroic ceramics prepared by a rapid liquid phase sintering method", *Ceram. Int*., **41**, (2015) 9285–9295.
11. J. Mata, A. Durán, E. Martínez, R. Escamilla, J. Heiras, J.M. Siqueiros, "Crystal structure and relaxor-type transition in $SrBi_2Ta_2O_9$ doped with praseodymium", *J. Phys. Condens. Matter*, **18** (2006) 10509.
12. H. Yan, Z. Zhang, W. Zhu, L. He, Y. Yu, C. Li, J. Zhou, "The effect of (Li,Ce) and (K,Ce) doping in Aurivillius phase material $CaBi_4Ti_4O_{15}$", *Mater. Res. Bull.*, **39** [9] (2004) 1237–1246.
13. M. Verma, A. Tanwar, K. Sreenivas, "Influence of lone pair on structural and electrical properties of Sb substituted Bismuth layered $SrBi_2Nb_2O_9$ ceramics", *Mater. Chem. Phys*., **209** (2018) 159–164.
14. D. Schütz, M. Deluca, W. Krauss, A. Feteira, T. Jackson, K. Reichmann, "Lone-pair-induced covalency as the cause of temperature- and field-induced instabilities in bismuth sodium titanate", *Adv. Funct. Mater*., **22** (2012) 2285–2294.
15. Zulhadjri, T.P. Wendari, M. Ikhram, Y.E. Putri, U. Septiani, Imelda, "Enhanced dielectric and ferroelectric responses in La^{3+}/Ti^{4+} co-substituted $SrBi_2Ta_2O_9$ Aurivillius phase", *Ceram. Int*., **48**, (2022) 10328–10332.
16. T.P. Wendari, S. Arief, N. Mufti, A. Insani, J. Baas, G. R. Blake, Zulhadjri, "Structure-property relationships in the lanthanide-substituted $PbBi_2Nb_2O_9$ Aurivillius phase synthesized by the molten salt method", *J. Alloys Compd*., **860** (2021) 158440.
17. M. Dhaou, E. Elaloui, K. Khirouni, H. Guermazi, S. Guermazi, "Enhancement of dielectric responses and conduction properties of Zn-doped TiO_2 for energy storage and photosensitivity applications", *J. Mater. Sci. Mater. Electron*., **32** (2021) 13187–13204.
18. S. Kumar, M. Panda, K. Manohor, S. Sahoo, R.N.P. Choudhary, "Impedance and modulus spectroscopic studies of lead free $Na_{1/2}Dy_{1/2}TiO_3$ ceramic", *Memories - Mater. Devices, Circuits Syst*., **2** (2022) 100013.
19. J.L. Izquierdo, G. Bolaños, V.H. Zapata, O. Morán, "Dielectric relaxation and ac conduction in multiferroic $TbMnO_3$ ceramics: Impedance spectroscopy analysis", *Curr. Appl. Phys*., **14** [11] (2014) 1492–1497.
20. K.S. Rao, D.M. Prasad, P. Murali Krishna, B.H.B. Suneetha, K. Suneetha, "Frequency and temperature dependence of electrical properties of barium and gadolinium substituted $SrBi_2Nb_2O_9$ ceramics", *J. Mater. Sci.*, **42** (2007) 7363–7374.
21. V. Senthil, T. Badapanda, A. Chandra Bose, S. Panigrahi, "Relaxation and conduction mechanism of Dy^{3+} substituted $SrBi_2Ta_2O_9$ ceramics", *J. Mater. Sci. Mater. Electron*.", **27** (2016) 4760–4770.